Microwave and Optical Entanglement for Quantum Transduction with Electro-Optomechanics

Changchun Zhong,[1,*] Xu Han,[2] and Liang Jiang[1]

[1] *Pritzker School of Molecular Engineering, University of Chicago, Chicago, Illinois 60637, USA*
[2] *Center for Nanoscale Materials, Argonne National Laboratory, Argonne, Illinois 60439, USA*

(Received 18 February 2022; revised 11 August 2022; accepted 28 October 2022; published 18 November 2022)

Quantum transduction refers to the coherent conversion between microwave and optical states, which can be achieved by quantum teleportation if given high-fidelity microwave-optical entanglement, namely entanglement-based quantum transduction. Reliable microwave-optical entanglement can be generated using various platforms. In this paper we base the discussion on a piezo-optomechanical system and make the teleportation induced conversion scheme more concrete in the framework of quantum channel theory. By comparing the quantum capacity between the entanglement-based conversion channel and the traditional direct quantum transduction channel, we show that the entanglement-based scheme indeed admits a positive transduction rate when the direct quantum transduction has zero quantum capacity. Given two piezo-optomechanical systems, we also investigate the generation of microwave-microwave entanglement from entanglement swapping within continuous-variable and discrete-variable settings, showing the potentials of directly connecting microwave quantum processors by microwave-microwave quantum teleportation.

DOI: 10.1103/PhysRevApplied.18.054061

I. INTRODUCTION

Distant microwave quantum processors, connected by efficient optical quantum channels, form an important design of quantum networks [1,2]. This design is appealing since it tries to combine two very different and important fields: (1) the superconducting circuit known for its advantages including efficient quantum control, hardware scalability, etc [3]; (2) the optical quantum channels for quantum information transmission with the feature of low communication loss, room-temperature quantum coherence preserving, etc [4,5]. Since optical and microwave photons do not interact, to build up this quantum network, a quantum transducer that coherently converts quantum information between microwave and optical frequencies is indispensable.

However, establishing such a quantum interface is extremely challenging to the state-of-the-art technology because the traditional *direct quantum transduction* (DQT), which linearly converts photons with beam-splitter-type coupling, requires both high coupling efficiency and small added noise [6–8]. Currently, DQT is being actively studied with various physical platforms, e.g., alkali atoms [9–11], rare-earth-doped crystals [12,13], electro-optomechanics [6,14–27], electro-optics [28–31], quantum magnonics [32,33], Rydberg atoms [34], etc. Although enormous progress has been made in the past several years for each platform (see the review article Ref. [35,36] and the cited references), all of them are still below the level, only above which direct quantum state conversion is possible.

Quantum state conversion can alternatively be realized by *entanglement-based quantum transduction* (EQT), which first generates microwave-optical (MO) entanglement with parametric down-conversion, then completes the state conversion through quantum teleportation [37,38]. Since a classical communication channel is used, EQT is expected to tolerate more noises and, thus, is less demanding in technical design. In fact, a series of recent studies already show the potential of high-fidelity MO entanglement generation based on the hybrid quantum systems in an experimental feasible regime [37,39,40], which paves the way for quantum transduction in the near term.

In this paper, based on the platform of piezo-optomechanics, we compare the performances of the same transducer working as EQT and DQT schemes. For DQT, we map out the system parameters where any quantum state conversion is impossible. While in the same parameter regime, we find the EQT still admits a finite quantum conversion rate, which is consistent with the result in quantum channel theory that a quantum channel with the assistance of classical communication could tolerate more noises [41,42]. It is noted that a recent work [43] shows

*zhong.changchun@uchicago.edu

a similar advantage based on a different electro-optic transducer model and with a different approach.

In addition, we discuss the generation of microwave-microwave (MM) entanglement by entanglement swapping with the entangled MO sources generated from two piezo-optomechanical systems [44,45]. The MM entanglement can be used to transmit microwave quantum information through teleportation induced channels, thus, directly connecting distant microwave circuits. Note this idea was suggested in Refs. [46–49] and later analyzed technically in the discrete-variable setting [50]. In this paper we further study this induced MM transmission channel and compare the corresponding MM entanglement generation rates between discrete and continuous variables.

In the sections that follow, we first introduce the piezo-optomechanical system, based on which the DQT and EQT schemes are compared in the framework of quantum channel theory. The transduction scheme from entanglement swapping is studied at the end. Throughout the paper, the convention $\hbar = 2$ is used for numerical calculations unless specified otherwise.

II. PIEZO-OPTOMECHANICS

We base our discussion on a piezo-optomechanical system, as shown schematically in Fig. 1. The thickness mode of a mechanical resonator is on the one hand coupled to the microwave mode through piezo-electricity, and on the other hand coupled to the optical mode by scattering pressure [51,52]. Denote $\hat{a}$, $\hat{b}$, and $\hat{c}$ as the optical, mechanical, and microwave mode operators, respectively, and ω_o, ω_m, and ω_e as the corresponding resonant frequencies. We use a laser with frequency ω_L to pump the optical mode and populate it with on average $\bar{n}_o$ photons. In the rotating frame of the laser, we can write down the linearized Hamiltonian of the system

$$\hat{H}/\hbar = -\Delta_o \hat{a}^\dagger \hat{a} + \omega_m \hat{b}^\dagger \hat{b} + \omega_e \hat{c}^\dagger \hat{c} - g_{em}(\hat{b}^\dagger \hat{c} + \hat{b}\hat{c}^\dagger) - g_{om,0}\sqrt{\bar{n}_o}(\hat{a}^\dagger + \hat{a})(\hat{b}^\dagger + \hat{b}), \quad (1)$$

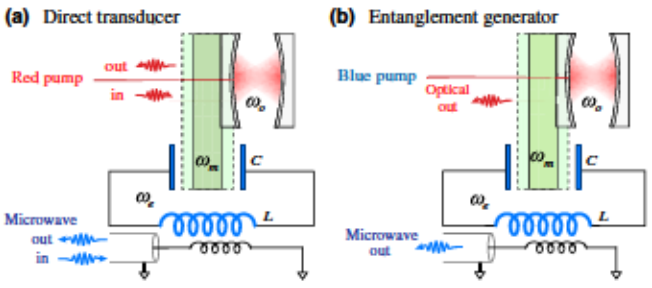

FIG. 1. Schematic figure for piezo-optomechanical system, used for (a) direct quantum transduction with a red detuned laser pump and for (b) an entanglement generator with a blue detuned laser pump.

where $\Delta_o = \omega_L - \omega_o$, g_{em} is the piezo-mechanical coupling strength and $g_{om,0}$ is the single-photon scattering pressure coupling, which can be enhanced by the cavity photons. The enhanced coupling strength is denoted as $g_{om} = g_{om,0}\sqrt{\bar{n}_o}$. Generally, in the piezo-optomechanical system, the mechanical resonator is intrinsically coupled to a thermal bath with a temperature around 10 millikelvin to 1 kelvin. For a several gigahertz mechanical resonator, the thermal noise can be routinely maintained around 1 [52,53]. Although this is already remarkable progress experimentally, as shown later, it is still challenging to demonstrate the quantum state conversion at the sub-photon level. In the following discussions we denote the intrinsic loss rate as κ_m for the mechanical mode and $\kappa_{e,I}$ for the microwave mode. The microwave mode also has a coupling port with loss rate $\kappa_{e,c}$. On the optical side, we denote the optical coupling and intrinsic loss rate as $\kappa_{o,c}$ and $\kappa_{o,I}$. Note the optical mode typically has a frequency in the terahertz regime, making the optical noise negligible even at room temperature and, thus, is neglected in later discussions.

III. DIRECT QUANTUM TRANSDUCTION

A. Piezo-optomechanical system for direct quantum transduction

Direct quantum transduction linearly converts quantum states coherently between the microwave and optical regime with the help of a beam-splitter-type interaction. This interaction can be generally obtained in many hybrid quantum systems [6,15,33]. For piezo-optomechanics, if we pump the optical mode in the red side band with $\Delta_o < 0$, the Hamiltonian Eq. (1) can be further simplified with rotating-wave approximation

$$\hat{H}/\hbar = -\Delta_o \hat{a}^\dagger \hat{a} + \omega_m \hat{b}^\dagger \hat{b} + \omega_e \hat{c}^\dagger \hat{c} + g_{om}(\hat{a}^\dagger \hat{b} + \hat{a}\hat{b}^\dagger) + g_{em}(\hat{b}^\dagger \hat{c} + \hat{b}\hat{c}^\dagger). \quad (2)$$

We see a beam splitter interaction is generated between the optical and mechanical modes, enabling the state conversion from optical to mechanical resonator and vice versa. The mechanical resonator further piezo-mechanically couples to the microwave mode and swaps the state between them, thus, indirectly realizing bidirectional microwave-optical transduction. [Note that when the system is on resonance $-\Delta_o = \omega_m = \omega_e$, the Hamiltonian can be further simplified in the rotating frame of ω_m as $\hat{H}/\hbar = g_{om}(\hat{a}^\dagger \hat{b} + \hat{a}\hat{b}^\dagger) + g_{em}(\hat{b}^\dagger \hat{c} + \hat{b}\hat{c}^\dagger)$. In this frame, the resonant frequency $\omega = 0$, which can enormously simplify the analytical expressions. This simplification will be used in all later discussions.] To quantify this conversion process in detail, we first write down the Heisenberg-Langevin

equations for each mode and the input-output relations as

$$\begin{aligned}\dot{\mathbf{a}} &= \mathbf{A}\mathbf{a} + \mathbf{B}\mathbf{a}_{\text{in}},\\ \mathbf{a}_{\text{out}} &= \mathbf{B}^T\mathbf{a} - \mathbf{a}_{\text{in}},\end{aligned} \tag{3}$$

where we label the vectors $\mathbf{a} = \{\hat{a}, \hat{c}, \hat{b}\}^T$, $\mathbf{a}_{\text{in}} = \{\hat{a}_{\text{in},c}, \hat{a}_{\text{in},i}, \hat{c}_{\text{in},c}, \hat{c}_{\text{in},i}, \hat{b}_{\text{in}}\}^T$, and $\mathbf{a}_{\text{out}} = \{\hat{a}_{\text{out},c}, \hat{a}_{\text{out},i}, \hat{c}_{\text{out},c}, \hat{c}_{\text{out},i}, \hat{b}_{\text{out}}\}^T$. The lower indexes "in" or "out" indicate the input and output modes, while "c" or "i" represent the coupling and intrinsic loss ports. Let matrices

$$\mathbf{A} = \begin{pmatrix} i\Delta_o - \frac{\kappa_o}{2} & 0 & -ig_{om} \\ 0 & -i\omega_e - \frac{\kappa_e}{2} & -ig_{em} \\ -ig_{om} & -ig_{em} & -i\omega_m - \frac{\kappa_m}{2} \end{pmatrix} \tag{4}$$

and

$$\mathbf{B} = \begin{pmatrix} \sqrt{\kappa_{o,c}} & \sqrt{\kappa_{o,i}} & 0 & 0 & 0 \\ 0 & 0 & \sqrt{\kappa_{e,c}} & \sqrt{\kappa_{e,i}} & 0 \\ 0 & 0 & 0 & 0 & \sqrt{\kappa_m} \end{pmatrix}. \tag{5}$$

The above equation group can be solved in the frequency domain by taking the Fourier transform $\hat{o}[\omega] = \int dt \hat{o}(t) e^{i\omega t}$, where $\hat{o}$ denotes an arbitrary operator. Straightforwardly, the input and output modes are shown to be connected by the scattering relation

$$\mathbf{a}_{\text{out}}[\omega] = \mathbf{S}[\omega] \cdot \mathbf{a}_{\text{in}}[\omega], \tag{6}$$

where $\mathbf{S}[\omega] = \mathbf{B}^T(-i\omega\mathbf{I}_3 - \mathbf{A})^{-1}\mathbf{B} - \mathbf{I}_5$. Based on the scattering matrix, we can identify the quantum transduction channel, e.g., with the on resonance condition ($\omega_m = \omega_e = -\Delta_o$), and the microwave to optical conversion channel that can be written as

$$\hat{a}_{\text{out},c} = \sqrt{\eta}\hat{c}_{\text{in},c} + \sqrt{1-\eta}\hat{e}, \tag{7}$$

which is interpreted as a beam splitter mixing the input signal and the thermal noise. The conversion efficiency η is

$$\eta = \frac{4C_{om}C_{em}}{(1 + C_{om} + C_{em})^2}\zeta_o\zeta_e. \tag{8}$$

Here $\zeta_o = \kappa_{o,c}/\kappa_o$ and $\zeta_e = \kappa_{e,c}/\kappa_e$ are the extraction ratios and the system cooperativities are given by $C_{om} = 4g_{om}^2/\kappa_o\kappa_m$ and $C_{em} = 4g_{em}^2/\kappa_e\kappa_m$. Note this efficiency is obtained for $\omega = 0$ that is optimal for a weakly coupled system [49]. The noise input operator $\hat{e}$ is defined as

$$\hat{e} = \frac{1}{\sqrt{1-\eta}}(S_{11}\hat{a}_{\text{in},c} + S_{12}\hat{a}_{\text{in},i} + S_{14}\hat{c}_{\text{in},i} + S_{15}\hat{b}_{\text{in}}). \tag{9}$$

If we ignore safely the optical noises, the average input noise photon is obtained,

$$n_e = \frac{1}{1-\eta}(|S_{14}|^2 n_c + |S_{15}|^2 n_b), \tag{10}$$

where $|S_{14}|^2 = \frac{4C_{em}C_{om}}{(1+C_{om}+C_{em})^2}\zeta_o(1-\zeta_e)$ and $|S_{15}|^2 = \frac{4C_{om}}{(1+C_{om}+C_{em})^2}\zeta_o$. In the piezo-optomechanical system, the mechanical mode and the microwave mode are intrinsically coupled to the same thermal bath with temperature $\mathcal{T}$, indicating $n_b = n_c = n_{\text{th}} \equiv (e^{\hbar\omega_m/k_B\mathcal{T}} - 1)^{-1}$. Thus, for a finite bath temperature, the microwave-optical conversion is a Bosonic thermal loss channel with transmissivity η and thermal noise n_e. We denote it as $\mathcal{N}(\eta, n_e)$ that maps an input state with covariance matrix $\mathbf{V}$ into $\mathbf{TVT}^T + \mathbf{N}$, where $\mathbf{T} = \sqrt{\eta}\mathbf{I}_2$ and $\mathbf{N} = (1-\eta)(2n_e+1)\mathbf{I}_2$ (see the appendix for a brief review of the Bosonic channel representation).

A channel is able to transmit quantum information as long as it has positive quantum channel capacity (see the appendix for a brief review). For many quantum channels including a thermal loss channel, finding their exact expressions of quantum capacity is hard. Instead, we resort to the capacity lower bound to study the channel properties. The channel $\mathcal{N}(\eta, n_e)$ admits a capacity lower bound [41]

$$\mathcal{Q}_{\text{LB}}^{\mathcal{N}} = \max\left\{0, \log_2\frac{\eta}{1-\eta} - g(n_e)\right\}, \tag{11}$$

where $g(x) \equiv (x+1)\log_2(x+1) - x\log_2 x$. Interestingly, this bound is tight for a so-called pure loss channel ($n_e = 0$). For a pure loss channel, it is easy to get that $\eta = 1/2$ is the threshold to have a positive channel capacity. Thus, for a thermal loss channel, it is necessary to have $\eta > 1/2$ in order to get a positive quantum capacity, since the thermal noise generally degrades the channel. Using this necessary condition and the expression Eq. (8), we have (noting that $\zeta_e\zeta_o \leq 1$)

$$C_{om}C_{em} > \left(\frac{1}{2\sqrt{2\zeta_o\zeta_e} - 2}\right)^2 \geq \frac{1}{(2\sqrt{2}-2)^2} \tag{12}$$

as the least requirement of the system to have a positive channel capacity. It is worth noting that this condition is not sufficient since the thermal noise as well as the nonunit extraction ratios could further degrade the channel behaviors. Currently, great effort is being put on designing and improving the experimental devices. Although huge

progress has been made in the past decade [7,8,52,54], the required parameter regime for positive capacity is still hard to reach with state-of-the-art technology.

IV. ENTANGLEMENT-BASED QUANTUM TRANSDUCTION

A. MO entanglement from piezo-optomechanical system

In Ref. [38] we proposed an entanglement-based quantum transduction scheme that first generates high-fidelity MO entanglement and then completes the quantum transduction by teleportation. The idea behind this is based on a well-known result in quantum channel theory: a very noisy channel can have positive quantum capacity with the assistance of a classical communication channel. In this section we make this idea more concrete based on the piezo-optomechanical system. We show the system is able to generate MO entanglement that induces an entanglement-based transduction channel with positive quantum capacity even when the system has zero capacity to perform any direct quantum transduction. Instead of using a red detuned laser, we pump the optical mode on the blue side band with $\Delta_o > 0$. Adopting the rotating-wave approximation, the Hamiltonian reads

$$\begin{aligned}\hat{H}/\hbar = &-\Delta_o \hat{a}^\dagger \hat{a} + \omega_m \hat{b}^\dagger \hat{b} + \omega_e \hat{c}^\dagger \hat{c} + g_{om}(\hat{a}^\dagger \hat{b}^\dagger + \hat{a}\hat{b}) \\ &+ g_{em}(\hat{b}^\dagger \hat{c} + \hat{b}\hat{c}^\dagger),\end{aligned} \tag{13}$$

where the optical and mechanical modes are driven in the parametric down-conversion regime and a two-mode squeezed state can be generated (similarly, the Hamiltonian can be further simplified with the system on resonant $\Delta_o = \omega_m = \omega_e$). Meanwhile the mechanical excitation can swap to the microwave mode through the piezo-electrical coupling, leading to an entangled MO output state. Ideally, the output entangled state is a two-mode squeezed vacuum, while in reality, the thermal noise and dissipation degrade it to a mixed two-mode squeezed Gaussian state. The output state can be obtained in a scattering picture, where the input Gaussian state (vacuum or thermal) is transformed into a Gaussian state under a Gaussian unitary. A Gaussian unitary is equivalently described by a symplectic transformation on the state quadrature [55]. Again, to obtain this transform, we first write down the Heisenberg-Langevin equation for each mode and combine the input-output relations

$$\begin{aligned}\dot{\mathbf{a}} &= \mathbf{M}\mathbf{a} + \mathbf{N}\mathbf{a}_{\text{in}}, \\ \mathbf{a}_{\text{out}} &= \mathbf{N}^T\mathbf{a} - \mathbf{a}_{\text{in}},\end{aligned} \tag{14}$$

where we group the operators into the vectors (similar to the previous section) $\mathbf{a}_{\text{in}} = (\hat{a}^\dagger_{\text{in},c}, \hat{a}^\dagger_{\text{in},f}, \hat{b}_{\text{in}}, \hat{c}_{\text{in},c}, \hat{c}_{\text{in},f})^T$, $\mathbf{a} = (\hat{a}^\dagger, \hat{b}, \hat{c})^T$, and $\mathbf{a}_{\text{out}} = (\hat{a}^\dagger_{\text{out},c}, \hat{a}^\dagger_{\text{out},f}, \hat{b}_{\text{out}}, \hat{c}_{\text{out},c}, \hat{c}_{\text{out},f})^T$. The resonance condition is taken ($\Delta_o = \omega_m = \omega_e$). Let matrices

$$\mathbf{M} = \begin{pmatrix} -\frac{\kappa_o}{2} & -ig_{om} & 0 \\ ig_{om} & -\frac{\kappa_m}{2} & ig_{em} \\ 0 & ig_{em} & -\frac{\kappa_e}{2} \end{pmatrix}, \tag{15}$$

$$\mathbf{N} = \begin{pmatrix} \sqrt{\kappa_{o,c}} & \sqrt{\kappa_{o,f}} & 0 & 0 & 0 \\ 0 & 0 & \sqrt{\kappa_m} & 0 & 0 \\ 0 & 0 & 0 & \sqrt{\kappa_{e,c}} & \sqrt{\kappa_{e,f}} \end{pmatrix}. \tag{16}$$

Taking the mode operators into the frequency domain, we find that $\mathbf{a}_{\text{out}} = \tilde{\mathbf{S}} \cdot \mathbf{a}_{\text{in}}$, where $\tilde{\mathbf{S}} = \mathbf{N}^T(-i\omega\mathbf{I}_3 - \mathbf{M})^{-1}\mathbf{N} - \mathbf{I}_5$. Using the relation

$$\begin{pmatrix} \hat{q} \\ \hat{p} \end{pmatrix} = \begin{pmatrix} 1 & 1 \\ -i & i \end{pmatrix} \begin{pmatrix} \hat{a} \\ \hat{a}^\dagger \end{pmatrix}, \tag{17}$$

we can convert the scattering matrix into the corresponding quadrature representation

$$\mathbf{x}_{\text{out}} = \mathbf{S} \cdot \mathbf{x}_{\text{in}}, \tag{18}$$

where $\mathbf{S}$ is the desired symplectic transform matrix. The vectors $\mathbf{x}_{\text{in/out}}$ collect all the input and output mode quadratures. If we label the two-mode (microwave and optical) output state quadratures as $\mathbf{x} = \{\hat{q}_o, \hat{p}_o, \hat{q}_e, \hat{p}_e\}^T$, a corresponding covariance matrix $\mathbf{V}^{\text{out}}_{oe}$ with the elements defined by $V_{ij} = 1/2\left\langle\{\hat{x}_i - \langle\hat{x}_i\rangle, \hat{x}_j - \langle\hat{x}_j\rangle\}\right\rangle$ can be obtained, and it can be expressed in the standard form

$$\mathbf{V}_{oe} = \begin{pmatrix} \mathbf{V}_A & \mathbf{V}_C \\ \mathbf{V}_C^T & \mathbf{V}_B \end{pmatrix}, \tag{19}$$

where $\mathbf{V}_A = u(\omega)\mathbf{I}_2, \mathbf{V}_C = w(\omega)\mathbf{Z}_2, \mathbf{V}_B = v(\omega)\mathbf{I}_2$. This matrix fully characterizes the output MO Gaussian state (ignoring the first moment of each mode since we only care about the state entanglement), where the diagonal elements $u(\omega), v(\omega)$ represent the corresponding output power spectrum densities and the element $w(\omega)$ indicates the quadrature correlations. Again, picking the resonant frequency ($\omega = 0$), the matrix elements can be simplified as

$$\begin{aligned} u &= 1 + \frac{8C_{om}[1 + N_{\text{th}} + C_{em}(1 + N_{\text{th}} - N_{\text{th}}\zeta_e)]\zeta_o}{(1 - C_{om} + C_{em})^2}, \\ v &= 1 + \frac{8[C_{em}(C_{om} + N_{\text{th}}) - (C_{om} - 1)^2(\zeta_e - 1)N_{\text{th}}]}{(1 - C_{om} + C_{em})^2\zeta_e^{-1}}, \\ w &= \frac{4[1 + C_{em} + C_{om} + 2N_{\text{th}}C_{om}(1 - \zeta_e) + 2N_{\text{th}}\zeta_e]}{(1 - C_{om} + C_{em})^2/\sqrt{C_{om}C_{em}\zeta_e\zeta_o}}. \end{aligned} \tag{20}$$

We shall show this state is indeed entangled in the following sections.

B. Teleportation induced transduction channel

With the MO entanglement generated from the piezo-optomechanics, bidirectional quantum transduction can be achieved using teleportation. In this section we show this entanglement-based conversion induces a Gaussian channel that can reach none zero quantum capacity in a large parameter space. Assume that we want to convert an input microwave state with covariance matrix $\mathbf{V}_{\text{in}}$ to the optical regime. According to the standard protocol [45,56,57], we first send the input mode and the microwave mode of the entangled source $\mathbf{V}_{oe}$ through a 50:50 beam splitter and perform a homodyne measurement to obtain p and q quadratures from the two outputs, respectively. Upon a conditional displacement, the input state can be recovered on the optical side.

The output state can be conveniently derived in the Wigner representation (see appendix for a brief review of the representation). Initially, we have a three-mode Wigner function up to normalization

$$W_I(\mathbf{x}) \propto e^{-\frac{1}{2}\mathbf{x}^T(\mathbf{V}_{oe}\oplus\mathbf{V}_{\text{in}})^{-1}\mathbf{x}}, \tag{21}$$

where $\mathbf{x} = (\mathbf{x}_o, \mathbf{x}_e, \mathbf{x}_{\text{in}})$. After the beam splitter, the homodyne measurement and the feed forward correction, the final Wigner function of the optical mode is given by

$$W_f(\mathbf{x}_o) \propto \int d\mathbf{x}_{\text{in}} d\mathbf{x}_e e^{-\frac{1}{2}\mathbf{x}^T[\mathbf{F}^T\mathbf{U}_{\text{BS}}^T(\mathbf{V}_{oe}\oplus\mathbf{V}_{\text{in}})^{-1}\mathbf{U}_{\text{BS}}\mathbf{F}]\mathbf{x}}, \tag{22}$$

where $\mathbf{U}_{\text{BS}}$ denotes the beam splitter unitary. The matrix $\mathbf{F}$ corresponds to the displacement operation that takes the form

$$\mathbf{F} = \begin{pmatrix} \mathbf{I}_2 & \sqrt{2}\mathbf{t}_1 & \sqrt{2}\mathbf{t}_2 \\ 0 & \mathbf{I}_2 & 0 \\ 0 & 0 & \mathbf{I}_2 \end{pmatrix}, \tag{23}$$

where $\mathbf{t}_1 = \kappa(\mathbf{I}_2 + \mathbf{Z}_2)/2$ and $\mathbf{t}_2 = \kappa(\mathbf{Z}_2 - \mathbf{I}_2)/2$, $\mathbf{Z}_2$ is the Pauli-z matrix and κ is an arbitrary gain factor. To identify the teleportation induced quantum channel, one can continue evaluating the integral. Instead, to avoid this tedious integral, we go to the characteristic function by Fourier transforming the Wigner function. Remembering a general Gaussian integral formula

$$\int d\mathbf{x} e^{-\mathbf{x}^T\mathbf{V}\mathbf{x}+\mathbf{x}^T\xi} \propto e^{\frac{1}{4}\xi^T\mathbf{V}^{-1}\xi}, \tag{24}$$

the output characteristic function can be shown to be specified by the first sub-block of the inverted matrix

$$[\mathbf{F}^T\mathbf{U}_{\text{BS}}^T(\mathbf{V}_{oe}\oplus\mathbf{V}_{\text{in}})^{-1}\mathbf{U}_{\text{BS}}\mathbf{F}]^{-1}, \tag{25}$$

which corresponds to the output covariance matrix. Straightforwardly, by picking out the first sub-block, we find the input covariance matrix is transformed as $\mathbf{V}_{\text{in}} \to \mathbf{T}\mathbf{V}_{\text{in}}\mathbf{T}^T + \mathbf{N}$ with

$$\begin{aligned} \mathbf{T} &= \kappa\mathbf{I}_2, \\ \mathbf{N} &= \mathbf{V}_A - \mathbf{V}_C\mathbf{Z}_2\mathbf{T} - (\mathbf{V}_C\mathbf{Z}_2\mathbf{T})^T + \mathbf{T}^T\mathbf{Z}_2\mathbf{V}_B\mathbf{Z}_2\mathbf{T} \\ &= (v\kappa^2 + u - 2w\kappa)\mathbf{I}_2. \end{aligned} \tag{26}$$

Obviously, this defines a single-mode Bosonic channel, e.g., when $\kappa < 1$, it mimics a thermal loss channel $\mathcal{N}'(\eta', n_e')$ with an effective transmissivity η' and effective thermal noise

$$\eta' = \kappa^2 < 1, \tag{27}$$

$$n_e' = \frac{v\kappa^2 + u - 2w\kappa}{2|1-\kappa^2|} - \frac{1}{2}. \tag{28}$$

Noting that the gain factor κ is arbitrary, the effective η' thus can be larger than 0.5, making a positive quantum capacity possible, as detailed in the next section. When the gain factor is chosen $\kappa > 1$, it mimics a thermal amplification channel $\mathcal{A}'(\eta', n_e')$ with $\eta' > 1$ and the thermal noise given by the same expression. Finally, when the modification constant $\kappa = 1$, it gives a random displacement channel with noise variance

$$\sigma^2 = v + u - 2w. \tag{29}$$

We denote this channel as $\mathcal{D}'(1, \sigma^2)$. Interestingly, the noise variance expression coincides with the term in the Duan criterion $v + u - 2w < 1$ [58], which sufficiently identifies the entanglement of a given continuous-variable quantum state. Intuitively, the smaller the term $u + v - 2w$ is, the more entangled the MO state is, and, thus, the smaller the noise variance is in the output of the teleportation induced conversion channel.

Similar to the thermal loss channel, the exact capacities of the thermal amplification channel and the random displacement channel are still not known. To quantify these channels, we use their lower bounds. For the thermal amplification channel, its lower bound has a similar form to the thermal loss channel and so can be put in the combined form

$$Q_{\text{LB}}^{\mathcal{N}',\mathcal{A}'} = \max\left\{0, \log_2\left(\frac{\kappa^2}{|1-\kappa^2|}\right) - g(n_e')\right\}. \tag{30}$$

For the random displacement channel, a transmission rate can be achieved by Gottesman-Kitaev-Preskill (GKP) code [59], which gives the quantum capacity lower bound

$$Q_{\text{LB}}^{\mathcal{D}'} = \max\left\{0, \log_2\left(\frac{2}{e\sigma^2}\right)\right\}. \tag{31}$$

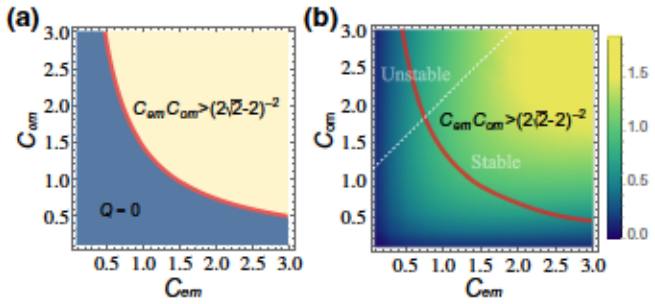

FIG. 2. (a) Direct quantum transduction behavior for a piezo-optomechanical system, where the red line separates the parameter regime between the quantum capacity is sure to be zero and the quantum capacity can possibly be positive. For the ideal case (zero thermal noise, unit extraction ratio), the red line becomes the exact quantum capacity threshold. (b) The capacity lower bound of the entanglement-based transduction channel in the ideal case (zero thermal noise, unit extraction ratio), showing a positive transduction rate in the regime where the direct transduction can only have zero capacity.

C. Entanglement-based conversion admits positive capacity with larger parameter space

In order to show the sharp contrast between DQT and EQT schemes, we first delineate the parameter regime for DQT capacity being zero and potentially nonzero in Fig. 2(a), then plot the quantum capacity of the EQT with ideal parameters (unit extraction ratio and zero bath noise; note that the effective noise is not zero) in Fig. 2(b). It shows EQT indeed has a positive quantum capacity in larger parameter regimes, even at the regime DQT is useless.

In Fig. 3 we plot the quantum capacity lower bound for more practical parameters, where the extraction ratios are fixed at $\zeta_o = 0.9, \zeta_e = 1$ and the thermal bath noise is slightly tuned. In Fig. 3(a) we take the cooperativities $C_{om} = C_{em} = 1$ (DQT useless regime even with no noise), where we see the EQT capacity lower bound could still be positive by tuning the gain constant κ and the channel can also tolerate certain bath noises. In Figs. 3(b) and 3(c) we scan the cooperativities C_{om} and C_{em} and get the optimized lower bound (picking the optimal κ) for bath noises $n_{\text{th}} = 0, 0.1$. Positive capacity is seen across the red curve to the lower left, where it is impossible for the DQT to transmit any quantum information. The fact that EQT has a larger parameter space for positive capacity will make the experimental design less demanding than DQT, which is quite appealing especially at this early stage of demonstrating quantum transduction.

The EQT channel consumes entanglement of the state generated from the piezo-optomechanical system. To show this state is indeed entangled, we calculate the two-mode Gaussian state entanglement of formation (E_F) [60] (see the appendix for the definition of entanglement of formation). As shown in Fig. 3(d), the E_F is positive at a large parameter regime, providing a good MO entanglement resource for teleportation. We see that the finite E_F indicates a positive capacity of the EQT channel, and E_F is generally larger than the capacity lower bound. The intuition is that the capacity lower bound is usually obtained from one-shot coherent information [61], which gives the one-shot distillable entanglement. E_F upper bounds the distillable entanglement, respecting the no-cloning theorem [62].

Lastly, it is worth mentioning that the system working in the parametric down-conversion regime could be unstable. The intuition is that when the blue detuned pump becomes too strong, the optomechanical parametric gain will be too large and cause instability. By checking the stability condition [39,63,64], we numerically identity the white dashed line separating the stable regime (lower right) from the unstable regime (upper-left corner), as shown both in Figs. 2 and 3.

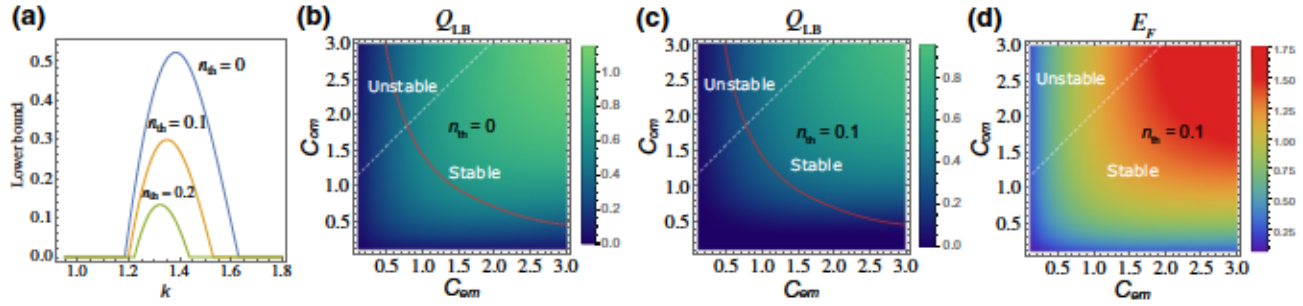

FIG. 3. (a) The quantum capacity lower bound of the teleportation induced conversion channel in terms of different gain constants, where the blue, orange, and green correspond to the piezo-optomechanical system with thermal bath $n_{\text{th}} = 0, 0.1$, and 0.2, respectively; (b),(c) are the capacity lower bound of the induced conversion channel in terms of system cooperativities for $n_{\text{th}} = 0, 0.1$, with each data optimized over the gain constant κ; (d) the E_F of the entangled MO state. In (b),(c),(d), the white dashed line divides the system from a stable (lower right) to unstable regime (up left). The red curves separate the parameter regime where direct transduction has zero capacity (lower left) or potentially positive capacity (upper right). In all plots, the extraction ratio $\zeta_o = 0.9, \zeta_e = 1$.

V. MICROWAVE-MICROWAVE ENTANGLEMENT FROM SWAPPING

A. Gaussian dynamics for entanglement swapping

The goal of quantum transduction is to connect distant microwave quantum processors. The above schemes achieve this goal by converting the signal to the optical regime, transmitting the optical photons through space and converting them back to microwaves. Alternatively, this same goal can be simplified if we have faithful MM entanglement, with which we can perform direct microwave signal transmission. Distant MM entanglement can be realized using two piezo-optomechanical systems, as shown in Fig. 4. The idea is to do *homodyne-based entanglement swapping*—projecting the optical modes onto an EPR state—where MM entanglement can be generated. In our setup, we can write down the two MO states as a four-mode Gaussian state $\mathbf{V}^1_{oe} \oplus \mathbf{V}^2_{oe}$, where $\mathbf{V}^{i=1,2}_{oe}$ are given by the output covariance matrix Eq. (19). The optical modes are then sent out for homodyne measurement and the initial entanglement is then expected to be swapped to the microwave modes.

To obtain the expression of the microwave entangled state, we briefly review the conditional Gaussian dynamics upon a general-dyne measurement on a portion of a given Gaussian state [44]. Suppose we have an initial Gaussian state with $n+m$ modes partitioned into A and B, respectively. The first moments for each mode are set to be zero and the covariance matrix is

$$\mathbf{V} = \begin{pmatrix} \mathbf{\Gamma}_A & \mathbf{\Gamma}_{AB} \\ \mathbf{\Gamma}^T_{AB} & \mathbf{\Gamma}_B \end{pmatrix}. \tag{32}$$

Then we perform a general-dyne measurement on the m modes of the system B. Depending on the measurement, one can get the conditional state of system A with n modes. A general-dyne measurement on the m modes is a set of positive operator-valued measurements, given by

$$\hat{F}_{\mathbf{r}_i} = \left\{ \frac{1}{(2\pi)^m} \hat{D}^{\dagger}_{\mathbf{r}_i} \rho_t \hat{D}_{\mathbf{r}_i} \right\}, \tag{33}$$

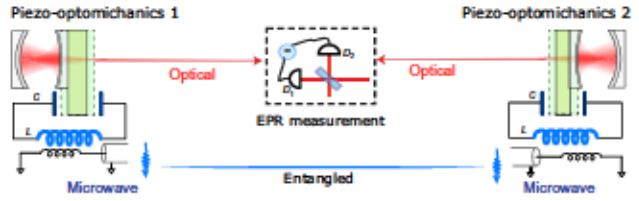

FIG. 4. Schematic figure for homodyne-based entanglement swapping scheme to generate microwave-microwave entanglement from two piezo-optomechanical systems. The photon click-based scheme can similarly be implemented by replacing the homodyne measurements in the middle by single-photon detections.

satisfying $\int_{R^{2m}} d\mathbf{r}_t \hat{F}_{\mathbf{r}_i} = \hat{I}$, where $\mathbf{r}_t \in R^{2m}$ is the measurement outcome and ρ_t is a Gaussian state with zero first moment and second moment $\mathbf{V}_t$. The probability of getting result $\mathbf{r}_t$ is given by

$$p(\mathbf{r}_t) = \frac{\exp(\mathbf{r}_t^T \frac{1}{\mathbf{\Gamma}_B + \mathbf{V}_t} \mathbf{r}_t)}{\pi^m \sqrt{\det(\mathbf{\Gamma}_B + \mathbf{V}_t)}}. \tag{34}$$

The state of the n modes of the subsystem A is mapped to [44]

$$\begin{aligned} \mathbf{V}^t_A &= \mathbf{\Gamma}_A - \mathbf{\Gamma}_{AB} \frac{1}{\mathbf{\Gamma}_B + \mathbf{V}_t} \mathbf{\Gamma}^T_{AB}, \\ \mathbf{r}^t_A &= \mathbf{\Gamma}_{AB} \frac{1}{\mathbf{\Gamma}_B + \mathbf{V}_t} \mathbf{r}_t, \end{aligned} \tag{35}$$

where we see a remarkable feature of the general-dyne conditioning: the conditional covariance matrix, which determines all correlations, does not depend on the measurement outcome.

We now apply this Gaussian conditioning to the entanglement swapping scheme, where we partition the four-mode state $\mathbf{V}^1_{oe} \oplus \mathbf{V}^2_{oe}$ into the optical (B) and microwave (A) part. With Eq. (19), we have $\mathbf{\Gamma}_A = v\mathbf{I}_4$, $\mathbf{\Gamma}_B = u\mathbf{I}_4$, and $\mathbf{\Gamma}_{AB} = \mathrm{diag}(w, -w, w, -w)$. The matrix $\mathbf{V}_t$ is first chosen to be a two-mode squeezed state

$$\mathbf{V}_t = \begin{pmatrix} \cosh(2r)\mathbf{I}_2 & \sinh(2r)\mathbf{Z}_2 \\ \sinh(2r)\mathbf{Z}_2 & \cosh(2r)\mathbf{I}_2 \end{pmatrix}, \tag{36}$$

then we take the limit $r \to \infty$ to simulate an ideal measurement. Finally, we obtain a covariance matrix

$$V_{\mathrm{MM}} = \begin{pmatrix} (v - \frac{w^2}{2u})\mathbf{I}_2 & \frac{w^2}{2u}\mathbf{Z}_2 \\ \frac{w^2}{2u}\mathbf{Z}_2 & (v - \frac{w^2}{2u})\mathbf{I}_2 \end{pmatrix}, \tag{37}$$

which determines the entanglement of the two-mode microwave state.

B. Entanglement for microwave information transmission

After the general-dyne measurement, we obtain a microwave two-mode Gaussian state given by Eq. (37), which is indeed entangled. It can be seen by evaluating the entanglement of formation, as shown in Fig. 5(a). This entanglement can be further used as a resource for teleportating quantum information encoded in microwave frequencies, inducing a direct microwave transmission channel. As we did in the previous section, we can similarly evaluate its quantum capacity lower bound, which is shown in Fig. 5(b). We pick the ideal case with extraction ratio $\zeta_o = \zeta_e = 1$ and the noise from the thermal bath $n_{\mathrm{th}} = 0$.

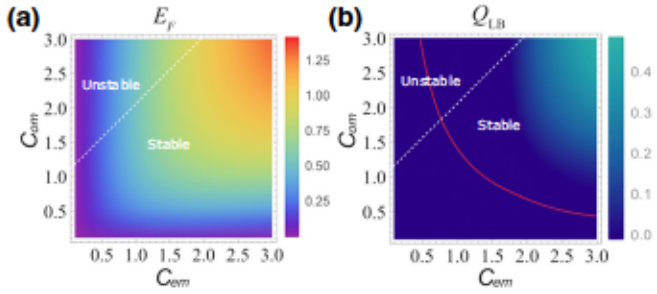

FIG. 5. (a) The entanglement of formation for the microwave-microwave state after the entanglement swap. (b) The quantum capacity lower bound of the teleportation induced transmission channel using the microwave-microwave entanglement. The white dashed line in each plot separates the piezo-optomechanical system between stable and unstable phases. The red solid line in (b) marks the boundary of the parameter regime where direct transduction has zero (lower left) or positive (upper right) capacity in the ideal case. In each plot, we set $\zeta_o = \zeta_e = 1$ and the thermal bath $n_{\text{th}} = 0$.

First, Fig. 5 shows that the teleportation induced MM transmission channel has a positive capacity lower bound only in the upper-right parameter regime, but not in the regime where DQT has zero capacity. Since the plot only shows the capacity lower bound, it is inconclusive whether the MM transmission channel outperforms the DQT channel or not, which requires further studies. Second, we see interestingly the quantum capacity lower bound is much smaller than the entanglement of formation. Since there is no bound entanglement in the two-mode Gaussian state [65], the capacity lower bound is very loose in this case. It would be interesting to better understand the structure of the entanglement in this entanglement swapping scheme and we shall leave this to future investigations.

VI. COMPARISON OF MM ENTANGLEMENT SWAPPING SCHEMES

The entanglement swapping can also be discussed in discrete variables similar to the well-known Duan-Lukin-Cirac-Zoller (DLCZ) scheme [50,66], where the system typically works at a very different parameter regime, e.g., entangled photon pairs can be generated by the weak parametric down-conversion. Also, we need the optical single-photon clicks to herald successful MM entanglement; thus, this *click-based entanglement swapping* scheme is generally probabilistic. While in the continuous variables, the continuous MM entanglement generation favors the strong parametric down-conversion regime and is usually nonprobabilistic due to the deterministic property of the homodyne measurement [44]. At the same time, we expect the MM entanglement from homodyne-based entanglement swapping to be more sensitive to optical photon loss error than that from the photon click-based protocol.

To make these comparison clear, we estimate their ability of entanglement generation from both schemes. For simplicity, we assume zero intrinsic thermal noises from all modes and the measurement devices are perfect for both protocols.

For the homodyne-based entanglement swapping scheme, the MM entanglement can be quantified by two-mode Gaussian entanglement of formation $E_F(\omega)$, which measures the amount of entanglement in the output state for a given frequency. In practice, it is important to check the entanglement within a certain bandwidth. Because of energy conservation, the overall output state is approximately in a tensor product of all frequency contributions, which indicates that the entanglement is additive. Thus, we define a quantity called entanglement of formation rate (E_R) as [49]

$$E_R = \frac{1}{2\pi}\int E_F(\omega)d\omega. \tag{38}$$

Intuitively, E_R tells how efficient a system is in generating entanglement. Since the entanglement of formation in general upper bounds is the distillable entanglement, the rate E_R actually gives an upper bound of the system's distillable entanglement rate [67]. For no optical photon loss, E_R depends on the MM state as given in Eq. (37). If we model an extra optical photon loss as a beam splitter with transmissivity τ, the MM state can be obtained by the replacement $u \to \tau(u-1)+1$ and $w \to \sqrt{\tau}w$, which generally results in a reduced entanglement rate.

In the click-based entanglement swapping protocol, optical single-photon detection is used to herald the entangled MM Bell pair (we assume photon-number resolving detectors). Since the optical mode is in a thermal state before it reaches the detector, the single-photon click statistics should follow the thermal distribution with probability $r_t\Delta t/(1+r_t\Delta t)^2$. Here Δt is the detection time window, which is typically chosen to be the transducer bandwidth of several microseconds, and r_t is the optical photon rate

$$r_t \equiv \langle \hat{a}^\dagger_{\text{out},c}\hat{a}_{\text{out},c}\rangle = \frac{1}{2\pi}\int \langle \hat{a}^\dagger_{\text{out},c}[\omega]\hat{a}_{\text{out},c}[\omega]\rangle\, d\omega. \tag{39}$$

Considering there are two piezo-optomechanical devices contributing to the optical heralding event, the single-photon *click rate* can be calculated by

$$r_B \simeq \frac{2r_t}{(1+r_t\Delta t)^2}, \tag{40}$$

which usually gives the heralded MM Bell state generation rate. Similarly, we can also model the optical photon loss by a beam splitter with transmissivity τ. As stated in the appendix, when this transmission loss is included, the heralded state is no longer a perfect Bell state. To estimate the

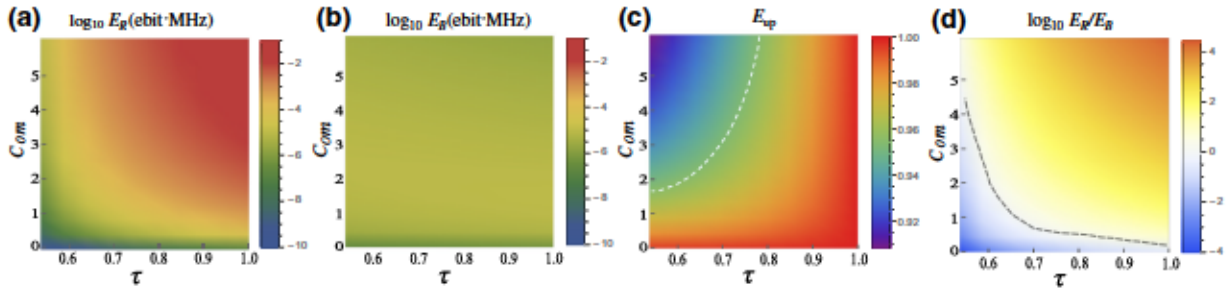

FIG. 6. (a) The entanglement of formation rate for the homodyne-based scheme and (b) the upper bound of entanglement of formation rate for the click-based scheme in terms of C_{om} and the optical transmissivity τ (both in same color scale). (c) Entanglement of formation upper bound of the photon click heralded MM state, which is strictly less than 1 ebit. The white dashed line separates the regimes, above (below) which the upper bound is smaller (larger) than 0.95 ebit. (d) The logarithm of the ratio E_R/E_B, where the black dashed line traces the points where the ratio $E_R/E_B = 1$. Above the line, the ratio is larger than one, indicating the continuous variable (CV) scheme is better. In each plot, we set $C_{em} = 10$, $\zeta_o = \zeta_e = 1$, and the thermal bath $n_{\rm th} = 0$. It is worth mentioning that the nonunit extraction ratios and thermal noise will degrade the entanglement rate for both schemes.

entanglement generation rate, one can calculate the heralded state's entanglement and then multiply that by the photon click rate. As detailed in the appendix, we obtain the upper bound of the heralded state's entanglement of formation ($E_{\rm up}$), which enables us to estimate the upper bound of the entanglement generation rate, denoted as E_B.

As shown in Fig. 6, we calculate the entanglement generation rate for both the homodyne-based protocol and click-based scheme. Figures 6(a) and 6(b) are in the same color scale. We see that the homodyne-based swapping scheme usually has a larger entanglement rate than the click-based protocol. Meanwhile, as expected, the homodyne-based swapping scheme favors the strong parametric down-conversion regime [the upper-right corner in Fig. 6(a) where C_{om} approaches C_{em}] and it is very sensitive to photon loss. In contrast, as shown in Fig. 6(b), the photon click-based scheme is much more robust to photon loss in generating entanglement. Also, it is preferred for the click-based scheme to work in the weak down-conversion regime (smaller C_{om}) since the single-photon pair generation is more probable. Figure 6(c) numerically plots the upper bound of entanglement of formation for the heralded MM state, where the white dashed line divides the parameter regimes into the upper (lower) part where the bound is smaller (larger) than 0.95 ebit. Obviously, higher optical transmission and weaker parametric down-conversion are favorable in generating pure entanglement. Note that $E_{\rm up}$ is still around 0.9 when the cooperativity and the transmission loss are large since higher photon excitation can contribute to the entanglement of formation, as indicated in Appendix E. Figure 6(d) plots the ratio E_R/E_B in log scale. The black dashed line traces the parameter regimes where $\log_{10} E_R/E_B = 0$, above which the CV scheme is better at generating entanglement. Below the line, the discrete variable (DV) scheme could potentially be advantageous over the CV scheme. In summary, the MM entanglement generation can be done in both discrete and continuous variables and we should properly choose the right protocol according to the practical requirements in the mission of quantum information transduction. For convenience, we summarize their difference in Table I.

VII. DISCUSSION

As discussed, EQT is in general more feasible for quantum state conversion that places much less demanding requirements on the physical implementations. To achieve the EQT, an important step is to successfully demonstrate the MO entanglement. As experimental technology develops, various physical systems, including piezo-optomechanics, electro-optics, etc., are reported to reach the EQT compatible regime, where high-fidelity entanglement could in principle be generated and quantified. In practice, e.g., for discrete-variable entanglement, the entanglement verification also requires efficient photon detection. Although an optical photon detector can already work with extremely high efficiency, microwave detection

TABLE I. Comparison of the photon click-based and the homodyne-based entanglement swapping schemes.

Click-based entanglement swapping	Homodyne-based entanglement swapping
- in photon-number basis	- in continuous-variable basis
- use single-photon detection	- use homodyne measurement
- probabilistic scheme with heralding	- deterministic scheme
- working in low squeezing regime	- working in high squeezing regime
- with detection of loss errors	

still suffers from limited sensitivity, thus hindering an efficient MO Bell measurement. Interestingly, with the help of circuit quantum electrodynamics for capturing microwave photons, it is shown that high-fidelity single microwave detection is possible [68]. We expect that as the experimental technique improves the MO entanglement should become more controllable, and the EQT would be the first quantum conversion scheme that coherently brings the two important fields—the optical communication channel and microwave quantum processor—together. In the mean time, distant MM entanglement from entanglement swapping would become more practical in coherently connecting quantum circuits. In short, these protocols together would bring the ambitious theoretical proposal of a quantum network more down to earth.

ACKNOWLEDGMENTS

C.Z. thanks Changhun Oh, Filip Rozpedek, especially Yuxin Wang for insightful discussions. C.Z. and L.J. acknowledge support from the ARO (W911NF-18-1-0020, W911NF-18-1-0212), ARO MURI (W911NF-16-1-0349, W911NF-21-1-0325), AFOSR MURI (FA9550-19-1-0399, FA9550-21-1-0209), AFRL (FA8649-21-P-0781), DoE Q-NEXT, NSF (OMA-1936118, EEC-1941583, OMA-2137642), NTT Research, and the Packard Foundation (2020-71479). X.H. acknowledges partial support from Argonne National Laboratory Directed Research and Development (LDRD) Program. Work performed at the Center for Nanoscale Materials, a U.S. Department of Energy Office of Science User Facility, was supported by the U.S. DOE, Office of Basic Energy Sciences, under Contract No. DE-AC02-06CH11357.

This is an expansion of the summary submitted to Optica Quantum 2.0 Conference. The submitted manuscript has been created by UChicago Argonne, LLC, Operator of Argonne National Laboratory ("Argonne"). Argonne, a U.S. Department of Energy Office of Science laboratory, is operated under Contract No. DE-AC02-06CH11357. The U.S. Government retains for itself, and others acting on its behalf, a paid-up nonexclusive, irrevocable worldwide license in said article to reproduce, prepare derivative works, distribute copies to the public, and perform publicly and display publicly, by or on behalf of the Government. The Department of Energy will provide public access to these results of federally sponsored research in accordance with the DOE Public Access Plan [71].

APPENDIX A: CHARACTERISTIC AND WIGNER FUNCTION OF GAUSSIAN STATE

Given any linear operator $\hat{o} \in \mathcal{L}(\mathcal{H})$ acting on the Hilbert space $\mathcal{H}$, one can define the p-norm of the operator as $||\hat{o}||_p \equiv [\mathrm{tr}\sqrt{\hat{o}^\dagger \hat{o}}^p]^{1/p}$. When $p = 2$, it is called the Hilbert-Schmidt norm, based on which one can define the Hilbert-Schmidt inner product for two operators

$$(\hat{o}_i|\hat{o}_j) \equiv \mathrm{tr}(\hat{o}_i^\dagger \hat{o}_j). \tag{A1}$$

If we confine the linear operator to the Heisenberg-Weyl group elements $\hat{D}_\xi \equiv \exp[-i\xi^T \Omega \hat{\mathbf{x}}]$ defined on n Bosonic modes, where $\xi \in \mathcal{R}^{2n}$, $\hat{\mathbf{x}} = \{\hat{q}_1, \hat{p}_1, \ldots, \hat{q}_n, \hat{p}_n\}^T$, and the Ω is the symplectic form

$$\mathbf{\Omega} \equiv \begin{pmatrix} 0 & 1 \\ -1 & 0 \end{pmatrix}^{\oplus n}, \tag{A2}$$

we have the orthogonality condition in terms of the Hilbert-Schmidt inner product

$$(\hat{D}_\xi|\hat{D}_\lambda) = (2\pi)^n \delta^{2n}(\xi - \lambda). \tag{A3}$$

Thus, we can view the Weyl operator as defining a set of operator basis elements, with which any other operator can be expanded. For instance, given a density operator ρ, it can be expanded according to

$$\rho = \frac{1}{(2\pi)^n} \int_{\mathcal{R}^{2n}} d^{2n}\xi \ \chi(\xi) \hat{D}_\xi, \tag{A4}$$

where the expansion coefficient $\chi(\xi)$ is typically named the characteristic function and $\chi(\xi) = (\hat{D}_\xi|\rho) = \mathrm{tr}(\hat{D}_\xi^\dagger \rho)$. Obviously, knowing the characteristic function is equivalent to knowing the state. The Wigner function is defined as the Fourier transform of the characteristic function

$$W(\mathbf{x}) = \frac{1}{(2\pi)^n} \int_{\mathcal{R}^{2n}} d^{2n}\xi \ \chi(\xi) e^{-i\mathbf{x}^T \Omega \xi}. \tag{A5}$$

For a Gaussian state with covariance matrix $\mathbf{V}$ and first moment $\bar{\mathbf{x}}$, one can show the characteristic function and the Wigner function take the form

$$\chi(\xi) = e^{-\frac{1}{2}\xi^T(\Omega \mathbf{V} \Omega^T)\xi - i(\Omega \bar{\mathbf{x}})^T \xi} \tag{A6}$$

and

$$W(\mathbf{x}) = \frac{e^{-\frac{1}{2}(\mathbf{x}-\bar{\mathbf{x}})^T \mathbf{V}^{-1}(\mathbf{x}-\bar{\mathbf{x}})}}{(2\pi)^n \sqrt{\det \mathbf{V}}}. \tag{A7}$$

APPENDIX B: QUANTUM CAPACITY AND GAUSSIAN CHANNEL

1. Coherent information

As capacity for the classical channel, quantum capacity is a quantity for measuring the channel's ability to transmit quantum information. In general, for many quantum channels, exactly knowing the quantum capacity is

hard. Instead, the lower or upper bound is used to partially describe the channels. In this appendix we discuss the lower bound—the coherent information—which defines an achievable rate of a channel to transmit quantum information.

In general, a quantum channel is defined by a completely positive and trace preserving (CPTP) map (the requirement of a quantum channel to be CPTP is nothing but keeping the quantum process physical)

$$\mathcal{N}: \rho_A \to \rho_B, \tag{B1}$$

where the system input is $\rho_A \in \mathcal{H}_A$ and the output $\rho_B \in \mathcal{H}_B$. Theoretically, any quantum channel has a unitary dilation defined as

$$\mathcal{N}(\rho_A) \equiv \mathrm{tr}_E[\mathcal{U}_{AE}(\rho_A \otimes |0\rangle\langle 0|_E)]. \tag{B2}$$

The subscript E is usually to denote the environment input (here we identify it with the output for simplicity). The above dilation naturally defines a complement channel

$$\mathcal{N}^c(\rho_A) \equiv \mathrm{tr}_A[\mathcal{U}_{AE}(\rho_A \otimes |0\rangle\langle 0|_E)]. \tag{B3}$$

Since unitary evolution usually correlates the system and the environment, the system output will not contain all the information of the input. The coherent information of a quantum channel is defined as

$$I_c(\mathcal{N}) \equiv \sup_{\rho_A}[S(\mathcal{N}(\rho_A)) - S(\mathcal{N}^c(\rho_A))], \tag{B4}$$

where $S(\rho) \equiv -\mathrm{tr}(\rho \log \rho)$ is the von Neumann entropy. The coherent information has a close connection with conditional entropy, which can be seen by adding an identity channel that acts on the purification of the system input. If we denote $|\psi\rangle_{RA}$ as a purification of ρ_A, we have a unitary channel $I_R \otimes \mathcal{U}_{AE}$ acting on the input $|\psi\rangle_{RA} \otimes |0\rangle_E$,

$$\rho_{RBE} = I_R \otimes \mathcal{U}_{AE}(|\psi\rangle_{RA} \otimes |0\rangle_E). \tag{B5}$$

Obviously, the output ρ_{RBE} is a pure state and the coherent information (maximized over the input ρ_A) can be written as

$$I_c(\mathcal{N}) = S(\rho_B) - S(\rho_{BR}), \tag{B6}$$

which is the negative conditional entropy of the state ρ_{RB}. Quantum conditional entropy being negative is a surprising quantum fact compared with classical probability theory, and we see interestingly it defines a lower bound of quantum capacity through the relation with coherent information.

Quantum capacity is defined as the optimal average coherent information when using the channel n times $Q \equiv \sup_n \frac{1}{n} I_c(\mathcal{N}^{\otimes n})$, which is generally difficult to calculate analytically. Since coherent information can be superadditive $I_c(\mathcal{N}_1 \otimes \mathcal{N}_2) \geq I_c(\mathcal{N}_1) + I_c(\mathcal{N}_2)$, the single-shot evaluation of coherent information usually provides a lower bound of the channel capacity.

2. Gaussian quantum channel

A Gaussian quantum channel can be specified by its action on the statistical first and second moments of an arbitrary Gaussian state $\hat{\rho}(\bar{\mathbf{x}}, \mathbf{V})$. In general, we have [69]

$$\begin{aligned} \bar{\mathbf{x}} &\to \mathbf{T}\bar{\mathbf{x}} + \mathbf{d}, \\ \mathbf{V} &\to \mathbf{T}\mathbf{V}\mathbf{T}^{\mathbf{T}} + \mathbf{N}, \end{aligned} \tag{B7}$$

where $\mathbf{T}, \mathbf{N}$ are real matrices satisfying the channel completely positive condition

$$\mathbf{N} + \mathbf{i}\Omega - \mathbf{i}\mathbf{T}\Omega\mathbf{T}^{\mathbf{T}} \geq 0. \tag{B8}$$

Here $\mathbf{d}$ is usually set to zero since it can be compensated by local displacement and is not affecting the state entanglement. Specifically, when $\mathbf{N} = \mathbf{0}$ and $\mathbf{T}$ is a symplectic matrix, it then defines a Gaussian unitary channel.

As stated in the main text, the thermal loss channel is modeled as a beam splitter mixing the input mode and the thermal noise

$$\mathbf{x} \to \sqrt{\eta}\mathbf{x}_{\mathrm{in}} + \sqrt{1-\eta}\mathbf{x}_{\mathbf{n_e}}. \tag{B9}$$

For a single-mode loss channel $\mathcal{N}(\eta, n_e)$, it is easy to verify that

$$\mathbf{T} = \sqrt{\eta}\mathbf{I}_2, \mathbf{N} = (1-\eta)(2n_e+1)\mathbf{I}_2, \tag{B10}$$

where $\eta < 1$ is the transmissivity and n_e denotes the thermal noise.

Similarly, for a single-mode thermal amplification channel $\mathcal{A}(\eta, n_e)$: $\mathbf{x} \to \sqrt{\eta}\mathbf{x}_{\mathrm{in}} + \sqrt{\eta-1}\mathbf{x}_{\mathbf{n_e}}$ with $\eta > 1$, we have

$$\mathbf{T} = \sqrt{\eta}\mathbf{I}_2, \mathbf{N} = (\eta-1)(2n_e+1)\mathbf{I}_2. \tag{B11}$$

The random displacement channel $\mathcal{D}(1, \sigma^2)$ can be considered as the limiting case of the above Bosonic channels, where the input signal is contaminated with random Gaussian noise with noise variance σ^2. We have

$$\mathbf{T} = \mathbf{I}_2, \mathbf{N} = \sigma^2\mathbf{I}_2. \tag{B12}$$

By investigating the coherent information of these Gaussian channels, we can lower bound their quantum capacities. For the single-mode thermal loss channel $\mathcal{N}(\eta, n_e)$ [or $\mathcal{A}(\eta, n_e)$], the lower bound is given by [41]

$$I_c(\mathcal{N}(\eta, n_e)) = \log_2\left|\frac{\eta}{1-\eta}\right| - g(n_e), \tag{B13}$$

where $g(x) = (x+1)\log_2(x+1) - x\log_2 x$. For the random displacement channel, a transmission rate can be

achieved using the GKP code [59], which gives the lower bound of quantum capacity, i.e.,

$$Q_{\mathrm{LB}}^{D'} = \max\left\{0, \log_2\left(\frac{2}{e\sigma^2}\right)\right\}. \tag{B14}$$

APPENDIX C: ENTANGLEMENT OF FORMATION

Entanglement of formation (E_F) of a general mixed bipartite state is defined as the infimum of the average von Neumann entropy taken over all its possible pure state decompositions

$$E_F = \inf_{p_i,|\psi\rangle} \sum_t p_t E(|\psi\rangle_t). \tag{C1}$$

It has been proven to be an effective entanglement measure for Gaussian states [60]. For a general two-mode Gaussian state, e.g., the output $\mathbf{V}_{oe}$ as specified in the text, a lower bound is given by the formula

$$E_F = \cosh^2 r \, \log_2\left(\cosh^2 r\right) - \sinh^2 r \, \log_2\left(\sinh^2 r\right), \tag{C2}$$

where r is the minimum amount of antisqueezing needed to disentangle the state

$$r = \frac{1}{4}\ln\left(\frac{\gamma - \sqrt{\gamma^2 - \beta_+\beta_-}}{\beta_-}\right), \tag{C3}$$

with

$$\begin{aligned}\gamma &= 2\left(\det \mathbf{V}_{oe} + 1\right) - (u(\omega) - v(\omega))^2,\\ \beta_\pm &= \det \mathbf{V}_A + \det \mathbf{V}_B - 2\det \mathbf{V}_C + 2u(\omega)v(\omega)\\ &\quad + 2w^2(\omega) \pm 4w(\omega)(u(\omega) + v(\omega)).\end{aligned} \tag{C4}$$

The lower bound is saturated for a two-mode Gaussian state in the standard form encountered in this paper. In the main text, we used the above formula to plot E_F with the on resonance frequency (taking $\omega = 0$).

APPENDIX D: BANDWIDTH LIMITED CHANNEL CAPACITY

In classical Shannon theory it is well known that the finite bandwidth of a transmission line gives a finite rate in data sampling [70], which places a constraint on the capacity rate. Similarly, any practical quantum transducer will have finite bandwidth, limiting the information transmission rate. In the expression Eq. (8) for the conversion efficiency, the on resonance frequency ($\omega = 0$) is chosen, while in general the conversion efficiency is given by

$$\eta(\omega) = \frac{4C_{om}C_{em}}{|C_{om}\alpha + C_{em}\beta + \alpha\beta\gamma|^2}\zeta_o\zeta_e, \tag{D1}$$

where $\alpha = 1 - 2i\omega/\kappa_e$, $\beta = 1 - 2i\omega/\kappa_o$, and $\gamma = 1 - 2i\omega/\kappa_m$. Note that this efficiency is defined according to $\eta(\omega) \equiv |\hat{a}_{\mathrm{out},c}(\omega)|^2/|\hat{c}_{\mathrm{in},c}(\omega)|^2$, where the ratio is between two power spectrum densities. Thus, the corresponding capacity Eq. (11) has a unit $[Q_{\mathrm{LB}}^{\mathcal{N}}(\omega)]$ =(ebit/s)/Hz. For a transducer with limited bandwidth, one can define a capacity rate that integrates all frequency contributions

$$Q_{\mathrm{LB}} \equiv \int d\omega Q_{\mathrm{LB}}^{\mathcal{N}}(\omega). \tag{D2}$$

This quantity has a unit $[Q_{\mathrm{LB}}^{\mathcal{N}}]$ = ebit/s, and it is also a lower bound. Since different quantum transducers generally have quite different transmission bandwidths, the capacity rate Q_{LB} defined above will be useful in comparing their different transduction abilities.

APPENDIX E: THE UPPER BOUND OF THE HERALDED ENTANGLEMENT OF FORMATION RATE FOR DV SCHEME

Even when one has a perfect single-photon detector, the single-photon click in the heralding scheme does not always herald a perfect Bell state if there is optical transmission loss. Instead, the state would be a mixed state. Intuitively, we might guess that the entanglement of the mixed state would be less than 1 ebit. Here, we show this intuition is correct.

Suppose the two transducers generate the product of a two-mode squeezed state (TMSS) $|\psi\rangle \otimes |\psi\rangle$, where $|\psi\rangle = \sum_n g_r(n)\,|n\rangle_o\,|n\rangle_e$ with $g_r(n) = \tanh^n r/\cosh r$. Note that if there is no transmission loss, the detector will get a thermal state with an average photon number $\sinh^2 r$. The single-photon click probability is given by $2g_r^2(1)$, which is also the probability of Bell state heralding.

The optical mode loss can be modeled as a beam splitter with transmissivity τ, which mixes an extra environment vacuum mode $\mathcal{E}$. After the beam splitter, each TMSS together with the environment state becomes $|\psi'\rangle = \sum_{n,k} f_{r,\tau}^{n,k}\,|k\rangle_o\,|n\rangle_e\,|n-k\rangle_{\mathcal{E}}$, where the coefficient $f_{r,\tau}^{n,k} = g_r(n)\sqrt{C_n^k}\tau^{k/2}(1-\tau)^{(n-k)/2}$ (C_n^k are binomial coefficients). With $|\psi'\rangle \otimes |\psi'\rangle$, clicking on one of the two detectors will herald the state $|\Psi\rangle = \sum_{n,n'} \phi_{n,n'} \otimes |n\rangle_{\mathcal{E}}\,|n'\rangle_{\mathcal{E}}$, where

$$\phi_{n,n'} = f_{r,\tau}^{n+1,1} f_{r,\tau}^{n',0}\,|n+1\rangle\,|n'\rangle + f_{r,\tau}^{n,0} f_{r,\tau}^{n'+1,1}\,|n\rangle\,|n'+1\rangle. \tag{E1}$$

(Note that if the detector is not single-photon-number resolving, there will be an extra term in the above equation $f_{r,\tau}^{n+1,1} f_{r,\tau}^{n'+1,1}\,|n+1\rangle\,|n'+1\rangle$, which will further degrade

the heralded state entanglement.) The final heralded MM state is obtained by tracing out the environment degree of freedom, which gives an ensemble of the above state

$$\Psi_{\mathrm{MM}} = \sum_{n,n'} P_{n,n'} \left|\tilde{\phi}_{n,n'}\right\rangle \left\langle\tilde{\phi}_{n,n'}\right|, \tag{E2}$$

where $\tilde{\phi}_{n,n'}$ is the normalized pure state. Since for a fixed pair n and n', $\tilde{\phi}_{n,n'}$ cannot have an entanglement larger than 1 ebit, the ensemble of them obviously can neither. Obviously, $|\Psi_{\mathrm{MM}}\rangle$ must be less entangled than a Bell state, matching our intuition. Thus, it is straightforward to see that the click rate should upper bound the heralded entanglement generation rate.

Because the heralded MM state Ψ_{MM} is in a specific decomposition of pure states, the corresponding entanglement should upper bound the state's entanglement of formation (note that entanglement of formation is obtained by minimizing all possible pure state decompositions), which in principle can be easily calculated. Multiplying this entanglement of formation upper bound by the single-photon click rate, we obtain the upper bound of the entanglement of formation rate, which is numerically shown in the main text.

[1] J. I. Cirac, P. Zoller, H. J. Kimble, and H. Mabuchi, Quantum State Transfer and Entanglement Distribution among Distant Nodes in a Quantum Network, Phys. Rev. Lett. **78**, 3221 (1997).

[2] H. J. Kimble, The quantum internet, Nature **453**, 1023 (2008).

[3] A. Blais, A. L. Grimsmo, S. M. Girvin, and A. Wallraff, Circuit quantum electrodynamics, Rev. Mod. Phys. **93**, 025005 (2021).

[4] W. Tittel, J. Brendel, H. Zbinden, and N. Gisin, Violation of Bell Inequalities by Photons More Than 10 km Apart, Phys. Rev. Lett. **81**, 3563 (1998).

[5] J. Yin *et al.*, Satellite-based entanglement distribution over 1200 kilometers, Science **356**, 1140 (2017).

[6] R. W. Andrews, R. W. Peterson, T. P. Purdy, K. Cicak, R. W. Simmonds, C. A. Regal, and K. W. Lehnert, Bidirectional and efficient conversion between microwave and optical light, Nat. Phys. **10**, 321 (2014).

[7] A. Vainsencher, K. J. Satzinger, G. A. Peairs, and A. N. Cleland, Bi-directional conversion between microwave and optical frequencies in a piezoelectric optomechanical device, Appl. Phys. Lett. **109**, 033107 (2016).

[8] M. Mirhosseini, A. Sipahigil, M. Kalaee, and O. Painter, Superconducting qubit to optical photon transduction, Nature **588**, 599 (2020).

[9] M. Hafezi, Z. Kim, S. L. Rolston, L. A. Orozco, B. L. Lev, and J. M. Taylor, Atomic interface between microwave and optical photons, Phys. Rev. A **85**, 020302(R) (2012).

[10] M. Kiffner, A. Feizpour, K. T. Kaczmarek, D. Jaksch, and J. Nunn, Two-way interconversion of millimeter-wave and optical fields in Rydberg gases, New J. Phys. **18**, 093030 (2016).

[11] B. T. Gard, K. Jacobs, R. McDermott, and M. Saffman, Microwave-to-optical frequency conversion using a cesium atom coupled to a superconducting resonator, Phys. Rev. A **96**, 013833 (2017).

[12] L. A. Williamson, Y.-H. Chen, and J. J. Longdell, Magneto-Optic Modulator with Unit Quantum Efficiency, Phys. Rev. Lett. **113**, 203601 (2014).

[13] C. O'Brien, N. Lauk, S. Blum, G. Morigi, and M. Fleischhauer, Interfacing Superconducting Qubits and Telecom Photons via a Rare-Earth-Doped Crystal, Phys. Rev. Lett. **113**, 063603 (2014).

[14] C. A. Regal and K. W. Lehnert, From cavity electromechanics to cavity optomechanics, J. Phys.: Conf. Ser. **264**, 012025 (2011).

[15] J. Bochmann, A. Vainsencher, D. D. Awschalom, and A. N. Cleland, Nanomechanical coupling between microwave and optical photons, Nat. Phys. **9**, 712 (2013).

[16] J. M. Taylor, A. S. Sørensen, C. M. Marcus, and E. S. Polzik, Laser Cooling and Optical Ddetection of Excitations in a *LC* Electrical Circuit, Phys. Rev. Lett. **107**, 273601 (2011).

[17] S. Barzanjeh, D. Vitali, P. Tombesi, and G. J. Milburn, Entangling optical and microwave cavity modes by means of a nanomechanical resonator, Phys. Rev. A **84**, 042342 (2011).

[18] Y.-D. Wang and A. A. Clerk, Using Interference for High Fidelity Quantum State Transfer in Optomechanics, Phys. Rev. Lett. **108**, 153603 (2012).

[19] L. Tian and H. Wang, Optical wavelength conversion of quantum states with optomechanics, Phys. Rev. A **82**, 053806 (2010); L. Tian, Adiabatic State Conversion and Pulse Transmission in Optomechanical Systems, Phys. Rev. Lett. **108**, 153604 (2012), doi:10.1103/PhysRevLett.108.153604; Optoelectromechanical transducer: Reversible conversion between microwave and optical photons, Ann. Phys. **527**, 1 (2014), doi:10.1002/andp.201400116.

[20] L. Midolo, A. Schliesser, and A. Fiore, Nano-opto-electro-mechanical systems, Nat. Nanotech. **13**, 11 (2018).

[21] T. Bagci, A. Simonsen, S. Schmid, L. G. Villanueva, E. Zeuthen, J. Appel, J. M. Taylor, A. Sørensen, K. Usami, A. Schliesser, and E. S. Polzik, Optical detection of radio waves through a nanomechanical transducer, Nature **507**, 81 (2014).

[22] M. Winger, T. D. Blasius, T. P. M. Alegre, A. H. Safavi-Naeini, S. Meenehan, J. Cohen, S. Stobbe, and O. Painter, A chip-scale integrated cavity-electro-optomechanics platform, Opt. Express **19**, 24905 (2011).

[23] A. Pitanti, J. M. Fink, A. H. Safavi-Naeini, J. T. Hill, C. U. Lei, A. Tredicucci, and O. Painter, Strong opto-electro-mechanical coupling in a silicon photonic crystal cavity, Opt. Express **23**, 3196 (2015).

[24] A. H. Safavi-Naeini and O. Painter, Proposal for an optomechanical traveling wave phonon–photon translator, New J. Phys. **13**, 013017 (2011).

[25] J. T. Hill, A. H. Safavi-Naeini, J. Chan, and O. Painter, Coherent optical wavelength conversion via cavity optomechanics, Nat. Commun. **3**, 1196 (2012).

[26] W. Jiang, R. N. Patel, F. M. Mayor, T. P. McKenna, P. Arrangoiz-Arriola, C. J. Sarabalis, J. D. Witmer, R. Van Laer, and A. H. Safavi-Naeini, Lithium niobate piezo-optomechanical crystals, Optica **6**, 845 (2019).

[27] W. Jiang, C. J. Sarabalis, Y. D. Dahmani, R. N. Patel, F. M. Mayor, T. P. McKenna, R. Van Laer, and A. H. Safavi-Naeini, Efficient bidirectional piezo-optomechanical transduction between microwave and optical frequency, Nat. Commun. **11**, 1 (2020).

[28] M. Tsang, Cavity quantum electro-optics, Phys. Rev. A **81**, 063837 (2010); Cavity quantum electro-optics. II. Input-output relations between traveling optical and microwave fields, Phys. Rev. A **84**, 043845 (2011), doi:10.1103/PhysRevA.84.043845.

[29] C. Javerzac-Galy, K. Plekhanov, N. R. Bernier, L. D. Toth, A. K. Feofanov, and T. J. Kippenberg, On-chip microwave-to-optical quantum coherent converter based on a superconducting resonator coupled to an electro-optic microresonator, Phys. Rev. A **94**, 053815 (2016).

[30] L. Fan, C.-L. Zou, R. Cheng, X. Guo, X. Han, Z. Gong, S. Wang, and H. X. Tang, Superconducting cavity electro-optics: A platform for coherent photon conversion between superconducting and photonic circuits, Sci. Adv. **4**, eaar4994 (2018).

[31] W. Fu, M. Xu, X. Liu, C.-L. Zou, C. Zhong, X. Han, M. Shen, Y. Xu, R. Cheng, S. Wang, L. Jiang, and H. X. Tang, Cavity electro-optic circuit for microwave-to-optical conversion in the quantum ground state, Phys. Rev. A **103**, 053504 (2021).

[32] R. Hisatomi, A. Osada, Y. Tabuchi, T. Ishikawa, A. Noguchi, R. Yamazaki, K. Usami, and Y. Nakamura, Bidirectional conversion between microwave and light via ferromagnetic magnons, Phys. Rev. B **93**, 174427 (2016).

[33] N. Zhu, X. Zhang, X. Han, C.-L. Zou, C. Zhong, C.-H. Wang, L. Jiang, and H. X. Tang, Waveguide cavity opto-magnonics for microwave-to-optics conversion, Optica **7**, 1291 (2020).

[34] J. Han, T. Vogt, C. Gross, D. Jaksch, M. Kiffner, and W. Li, Coherent Microwave-to-Optical Conversion via Six-Wave Mixing in Rydberg Atoms, Phys. Rev. Lett. **120**, 093201 (2018).

[35] N. Lauk, N. Sinclair, S. Barzanjeh, J. P. Covey, M. Saffman, M. Spiropulu, and C. Simon, Perspectives on quantum transduction, Quantum Sci. Technol. **5**, 020501 (2020).

[36] X. Han, W. Fu, C.-L. Zou, L. Jiang, and H. X. Tang, Microwave-optical quantum frequency conversion, Optica **8**, 1050 (2021).

[37] S. Barzanjeh, M. Abdi, G. J. Milburn, P. Tombesi, and D. Vitali, Reversible Optical-to-Microwave Quantum Interface, Phys. Rev. Lett. **109**, 130503 (2012).

[38] C. Zhong, Z. Wang, C. Zou, M. Zhang, X. Han, W. Fu, M. Xu, S. Shankar, M. H. Devoret, H. X. Tang, and L. Jiang, Proposal for Heralded Generation and Detection of Entangled Microwave–Optical-Photon Pairs, Phys. Rev. Lett. **124**, 010511 (2020).

[39] L. Tian, Robust Photon Entanglement via Quantum Interference in Optomechanical Interfaces, Phys. Rev. Lett. **110**, 233602 (2013).

[40] A. Rueda, W. Hease, S. Barzanjeh, and J. M. Fink, Electro-optic entanglement source for microwave to telecom quantum state transfer, Npj Quantum Inf. **5**, 1 (2019).

[41] C. Weedbrook, S. Pirandola, R. García-Patrón, N. J. Cerf, T. C. Ralph, J. H. Shapiro, and S. Lloyd, Gaussian quantum information, Rev. Mod. Phys. **84**, 621 (2012).

[42] R. García-Patrón, S. Pirandola, S. Lloyd, and J. H. Shapiro, Reverse Coherent Information, Phys. Rev. Lett. **102**, 210501 (2009).

[43] J. Wu, C. Cui, L. Fan, and Q. Zhuang, Deterministic Microwave-Optical Transduction Based on Quantum Teleportation, Phys. Rev. Appl. **16**, 064044 (2021).

[44] A. Serafini, *Quantum Continuous Variables: a Primer of Theoretical Methods* (CRC press, 2017).

[45] A. Furusawa, J. L. Sørensen, S. L. Braunstein, C. A. Fuchs, H. J. Kimble, and E. S. Polzik, Unconditional quantum teleportation, Science **282**, 706 (1998).

[46] M. Abdi, S. Pirandola, P. Tombesi, and D. Vitali, Entanglement Swapping with Local Certification: Application to Remote Micromechanical Resonators, Phys. Rev. Lett. **109**, 143601 (2012).

[47] M. Abdi, S. Pirandola, P. Tombesi, and D. Vitali, Continuous-variable-entanglement swapping and its local certification: Entangling distant mechanical modes, Phys. Rev. A **89**, 022331 (2014).

[48] M. Abdi, P. Tombesi, and D. Vitali, Entangling two distant non-interacting microwave modes, Ann. Phys. **527**, 139 (2015).

[49] C. Zhong, X. Han, H. X. Tang, and L. Jiang, Entanglement of microwave-optical modes in a strongly coupled electro-optomechanical system, Phys. Rev. A **101**, 032345 (2020).

[50] S. Krastanov, H. Raniwala, J. Holzgrafe, K. Jacobs, M. Lončar, M. J. Reagor, and D. R. Englund, Optically Heralded Entanglement of Superconducting Systems in Quantum Networks, Phys. Rev. Lett. **127**, 040503 (2021).

[51] M. Aspelmeyer, T. J. Kippenberg, and F. Marquardt, Cavity optomechanics, Rev. Mod. Phys. **86**, 1391 (2014).

[52] X. Han, W. Fu, C. Zhong, C.-L. Zou, Y. Xu, A. Al Sayem, M. Xu, S. Wang, R. Cheng, L. Jiang, and Hong X. Tang, Cavity piezo-mechanics for superconducting-nanophotonic quantum interface, Nat. Commun. **11**, 1 (2020).

[53] M. Xu, X. Han, C.-L. Zou, W. Fu, Y. Xu, C. Zhong, L. Jiang, and H. X. Tang, Radiative Cooling of a Superconducting Resonator, Phys. Rev. Lett. **124**, 033602 (2020).

[54] A. P. Higginbotham, P. Burns, M. Urmey, R. Peterson, N. Kampel, B. Brubaker, G. Smith, K. Lehnert, and C. Regal, Harnessing electro-optic correlations in an efficient mechanical converter, Nat. Phys. **14**, 1038 (2018).

[55] M. A. De Gosson, *Symplectic Geometry and Quantum Mechanics* (Springer Science & Business Media, 2006), Vol. 166.

[56] S. Pirandola and S. Mancini, Quantum teleportation with continuous variables: A survey, Laser Phys. **16**, 1418 (2006).

[57] S. Pirandola, J. Eisert, C. Weedbrook, A. Furusawa, and S. L. Braunstein, Advances in quantum teleportation, Nat. Photonics **9**, 641 (2015).

[58] L.-M. Duan, G. Giedke, J. I. Cirac, and P. Zoller, Inseparability Criterion for Continuous Variable Systems, Phys. Rev. Lett. **84**, 2722 (2000).

[59] D. Gottesman, A. Kitaev, and J. Preskill, Encoding a qubit in an oscillator, Phys. Rev. A **64**, 012310 (2001).

[60] S. Tserkis and T. C. Ralph, Quantifying entanglement in two-mode Gaussian states, Phys. Rev. A **96**, 062338 (2017).

[61] B. Schumacher and M. A. Nielsen, Quantum data processing and error correction, Phys. Rev. A **54**, 2629 (1996).

[62] P. M. Hayden, M. Horodecki, and B. M. Terhal, The asymptotic entanglement cost of preparing a quantum state, J. Phys. A: Math. Gen. **34**, 6891 (2001).

[63] E. X. DeJesus and C. Kaufman, Routh-Hurwitz criterion in the examination of eigenvalues of a system of nonlinear ordinary differential equations, Phys. Rev. A **35**, 5288 (1987).

[64] Y.-D. Wang, S. Chesi, and A. A. Clerk, Bipartite and tripartite output entanglement in three-mode optomechanical systems, Phys. Rev. A **91**, 013807 (2015).

[65] G. Giedke, L.-M. Duan, J. I. Cirac, and P. Zoller, All inseparable two-mode Gaussian continuous variable states are distillable, arXiv preprint arXiv:quant-ph/0007061 (2000).

[66] L.-M. Duan, M. D. Lukin, J. I. Cirac, and P. Zoller, Long-distance quantum communication with atomic ensembles and linear optics, Nature **414**, 413 (2001).

[67] Y. Guo, Strict entanglement monotonicity under local operations and classical communication, Phys. Rev. A **99**, 022338 (2019).

[68] P. Campagne-Ibarcq, E. Zalys-Geller, A. Narla, S. Shankar, P. Reinhold, L. Burkhart, C. Axline, W. Pfaff, L. Frunzio, R. J. Schoelkopf, and M. H. Devoret, Deterministic Remote Entanglement of Superconducting Circuits through Microwave Two-Photon Transitions, Phys. Rev. Lett. **120**, 200501 (2018).

[69] J. Eisert and M. M. Wolf, Gaussian quantum channels, arXiv preprint arXiv:quant-ph/0505151 (2005).

[70] C. E. Shannon, Communication in the presence of noise, Proc. IRE **37**, 10 (1949).

[71] http://energy.gov/downloads/doe-public-access-plan